Geophysical Research Letters

RESEARCH LETTER
10.1029/2019GL082198

Source Localization of Microseismic Emissions During Pneumatic Fracturing

Antoine L. Turquet[1,2,3], Renaud Toussaint[1,2,3], Fredrik Kvalheim Eriksen[1,2,3], Guillaume Daniel[4], Olivier Lengliné[1,3], Eirik G. Flekkøy[2,3], and Knut Jørgen Måløy[2,3]

[1]Institut de Physique du Globe de Strasbourg, UMR7516, University of Strasbourg/EOST, CNRS, Strasbourg, France, [2]SFF PoreLab, Njord Centre, Department of Physics, University of Oslo, Oslo, Norway, [3]International Associate Laboratory LIA D-FFRACT, Deformation, Flow and Fracture of Disordered Materials, Oslo, Norway, [4]EDF-Direction Industrielle, Aix-en-Provence, France

Abstract Localization of signals is a widely applied technique used in different areas of science telecommunication, medicine, or seismology. In this work, we study microseismic emissions due to stick-slip events during pneumatic fracture in a transparent setup at laboratory scale and apply a localization method "Estimated Source Energy Homogeneity." The seismic location results are compared with the image correlation results for displacement maps corresponding to the event times. We have observed (using optics and acoustics) that the movement starts inside the porous medium and progresses toward the channel tips, eventually causing channels to grow further. This finding could be of interest in understanding fluid-induced earthquake nucleation processes. Similar to in-site applications of pneumatic or fluid-related fracturing, it shows that the area influenced extends beyond the fracture tips. This also shows why even after the end of pumping, we may get earthquakes, such as in the Basel case (Haring et al., 2008, https://doi.org/10.1016/j.geothermics.2008.06.002).

Plain Language Summary An uncompacted granular medium having a fixed grain size is placed between two glass plates as a very thin layer. Using air injection, this porous medium is compacted and fractured. This system is monitored using a camera capable of recording more than 100 images per second and accelerometers which can record vibrations in high frequencies. During this injection, earthquake-like vibrations are generated by the system. Sources of these vibrations are located using acoustic recordings and image processing. We have observed that the channeling starts with a compaction inside the medium; this compaction propagates toward the channel tips and cause them to advance further inside the medium.

Key Points:
- Pneumatic fracturing experiments in a Hele-Shaw cell are monitored using accelerometers and a high-speed camera
- Acoustic emissions are localized using an energy-based signal location method, and displacement maps are obtained from image correlation
- By comparing the acoustic and the optical results, we observe that motion starts within porous medium and propagates toward the channel tips

Supporting Information:
- Supporting Information S1

Correspondence to:
A. L. Turquet,
turquetal@gmail.com

Citation:
Turquet, A. L., Toussaint, R., Eriksen, F. K. K., Daniel, G., Lengliné, O., Flekkøy, E. G., & Måløy, K. J. (2019).Source localization of microseismic emissions during pneumatic fracturing. *Geophysical Research Letters*, *46*. https://doi.org/10.1029/2019GL082198

Received 29 JAN 2019
Accepted 27 FEB 2019
Accepted article online 4 MAR 2019

1. Introduction

Acoustic signal localization is applied in many different areas of science (Elnahrawy et al., 2004; Gershman et al., 1995; Garnier & Fink, 2015; Fink, 2015; Malioutov et al., 2005; Valin et al., 2003; Zhu et al., 2007). In robotics, speech source tracking is done to automate cameras to follow the speaker (Brandstein et al., 1997). In electronics, touch screens are a very popular example of a signal localization. It is necessary for the system to locate the touch of a user to transmit information to process a simple message (Terlizzi & Minoo, 2009).

Similarly, in earth sciences, finding the epicenter of an earthquake is necessary to understand how it was generated, where exactly the movement occurred, and which region is more risky for the aftershocks (Aki & Richards, 2002). For a better quality risk assessment, it is important to know the origin of the seismicity along with its location. In nature, seismic events based on gas-solid interactions are very common. For example, there are many existing studies about a volcano-heated fluid that becoming gas and causing phreatic eruptions or geysers (Christenson et al., 2010; Jolly et al., 2014; Manga & Brodsky, 2006; Oppenheimer, 1986; Sudo et al., 1998; Tazieff, 1989). Moreover, fast air or fluid injection deforming porous medium is used in industrial applications of pneumatic fracturing (Accutech, 1994; Gao et al., 2014; Schuring et al., 1996) or hydraulic fracturing (Aochi et al., 2011; Charléty et al., 2007; Cuenot et al., 2008; Dorbath et al., 2009). At very large scales (tens or hundreds of meters) and high-pressure injection, compressibility plays a role in the interactions between the pressurized fluid and deformable solid medium similar to the gas-solid interactions mentioned earlier. This physical phenomenon can be observed in magma fracturing, eruptions

(Poland et al., 2012; Rivalta & Segall, 2007), fluid injection into rocks, or reservoir stimulations in geothermal fields (Candela et al., 2018). Stanchits et al. (2011) have studied the acoustic emissions on rock samples during thermo-hydro-chemo-mechanical coupled deformations. Water injection into porous sandstone under applied stress induced acoustic emission events. These events are generated close to the migrating waterfront. Kobchenko et al. (2013) studied the transport of CO_2 by diffusion and fracturing the gel layer in a Hele-Shaw cell. They studied the length scales of diffusion and flow in fracture networks, which are eventually linked to statistical properties of river networks and hierarchical-fracture networks. In the very recent research of Jamtveit et al. (2018), they have found that the strike-slip lower crust earthquakes are causing fluid pressure pulses toward the lower crust and fluid-driven associated metamorphic and structural transformations of this zone follow these earthquakes. More importantly, at large scales, a common way to understand and control the fluid-induced fracturing is to monitor the microseismicity (Cornet et al., 1998; Cornet, 2015; Fehler et al., 1987; Holland, 2013; Valkó & Economides, 1995). The source locations of seismic events are mainly focusing on the fluid-solid coupled events.

Even though the localization of the microseismicity due to volcanoes and industrial applications (e.g. hydraulic fracturing) have very rich scientific literature, the locations of acoustic emissions based on interactions between the injected gas and deformable solid (or gas-metal in pressure tanks, Peacock, 1996) remain challenging. To the best of our knowledge, acoustic emissions have not been studied during pneumatic fractures in the scientific literature prior to this article. In this article, we are investigating the source mechanisms and locations of pneumatic fractures in a porous medium in a transparent Hele-Shaw cell. The main focus of this work is to first locate the stick-slip events using acoustic emissions and then to compare them with the displacement field obtained from digital image correlation. The main reason behind using a Hele-Shaw cell is to optically record the deformations associated with the microseismic event while recording the vibrations on the glass plate with accelerometers. This work is based on an experimental approach similar to Turkaya et al. (2015), Eriksen et al. (2017), Eriksen et al. (2018), and Turquet et al. (2018).

Some of the signal localization types have been recently reviewed in Turkaya et al. (2016). In the present article, we show the application of the estimation of source energy homogeneity (ESEH) to locate the source of the acoustic emissions during aerofracturing experiments (Turkaya et al., 2015). These localization results are compared with the Digital Image Correlation (DIC; details can be found in Eriksen et al. (2018) results), as obtained from the optical recordings via a high-speed camera during the experiment.

2. Experimental Setup

The aerofracturing experiments analyzed here are conducted in a Hele-Shaw cell made of two glass plates 80 cm × 40 cm × 1 cm with an aperture of 1 mm between them—see details in Turkaya et al. (2015), Eriksen et al. (2017), Eriksen et al. (2018), and Turquet et al. (2018). The experimental setup is shown in Figure 1a. The acquisition chains of optical and acoustic data are presented. The system is triggered via a signal generator to have synchronization between optical and acoustic data. The optical data were recorded at 125 or 1,000 images per second using a Photron SA5 and a flicker-free Dedolight 400-W projector, and for acoustic data, we use 1-MHz sampling rate. Three boundaries of this cell are sealed with a double-sided tape, while the fourth side is covered with a 40-μm mesh filter. This filter lets the air pass to the surrounding atmosphere while keeping the grains inside the cell. In this particular experiment, we used 1-bar overpressure from the inlet and we used 80-μm grains having material density 1.05 g/cm^3 in loose state inside the cell. Prior to the experiment, the cell is filled vertically before sealing with a semipermeable mesh. Then, the cell is rotated vertically so that the grains fall freely to the other end of the cell. This leads to solid ratio be very close to the random loose packing with a solid fraction of $\phi = 0.44 \pm 0.04$ (Eriksen et al., 2017). Finally, the cell is carefully placed horizontally without affecting this loose state. This simple preparation procedure ensures that the experiments are reproducible. An empty space is provided between the air inlet and the solid-air interface to provide a homogenous pressure over the width of the cell. The air overpressure at the inlet is then raised and maintained at a constant level (1 bar in the example on Figure 1).

During this experiment, acoustic signals are recorded using four accelerometers attached to the bottom plate (see Figure 1b). The sensors are placed toward the outlet (where most of the stick-slip events are happening) to have a better signal resolution. The sensors are miniature piezoelectric charge accelerometer 4374—Brüel & Kjaer associated to a NEXUS Charge Amplifier—Type 2692-A conditioner, and the signal is digitized using a National Instruments NI-DAQ mx acquisition card PCI-6133 8 Channels acquisition card. The accelerome-

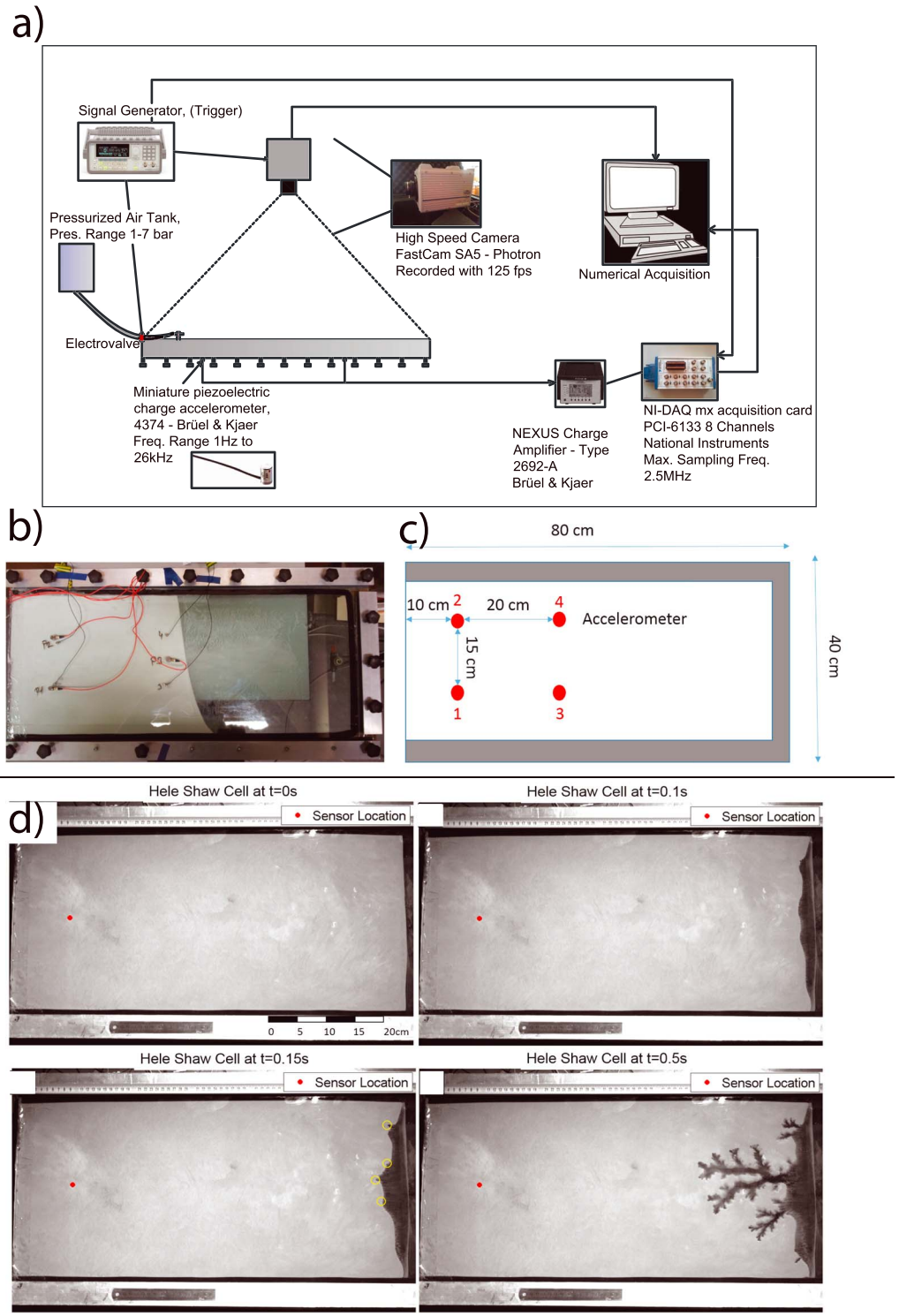

Figure 1. (a) The acquisition chain of the aerofracturing experiments with a Hele-Shaw cell. The signal acquisition card, camera, and the electrovalve connected to the air pump are triggered at the same time via a Transistor-Transistor Logic (TTL) signal sent from the signal generator to have synchronized optical and acoustic data. The sensors are placed on the bottom glass plate of the Hele-Shaw cell using a solid crystallized phenyl salicylate. (b) The image showing the accelerometers stick under the Hele-Shaw cell is given. In (c), accelerometers are sketched and numbered. Red dots show the positions of the accelerometers. (d) We present several snapshots of the cell during injection.

ters have 1 Hz to 26 kHz flat response. Using the function given by the manufacturer the response is flattened up to 200 kHz. These accelerometers can detect plate motions normal to the glass plate surface only. Depending on the sign of the cumulative displacement (positive or negative) recorded at the sensor we mark the corresponding signals with the polarization up or down, respectively. The acoustic events are located using ESEH for a certain window of the signal which starts at the arrival time and ends somewhere in the coda. We have presented a more detailed discussion linking the acoustic signal polarization to medium deformation in Text S1 of the supporting information. More information about time windowing can be obtained from Supplementary Figure S1 and associated caption. Furthermore, the procedure of detecting the acoustic events from raw recordings is described in Text S2.

3. The ESEH

ESEH considers that the source energy calculated from different recordings should be the same after the correction of energy loss due to the travel path attenuation (based on material and distance). Let E_s be the energy of the source and assume that the energy spread cylindrically on the plates. In that case, the recorded energy E_n at receiver n at a distant R can be expressed as $E_n = \frac{E_s}{2\pi Rh}$, where h is the plate thickness. E_s can be estimated following Farin et al. (2016), Hibert et al. (2011), and Turkaya et al. (2016) by

$$E_s(\mathbf{r_s}, \mathbf{r_n}) = \int_0^{\omega_{Nyq}} 2\pi R(n)\rho hc(\omega)\frac{|a(\omega)|^2}{\omega^2}\mathrm{d}\omega, \tag{1}$$

where $E_s(r_s, r_n)$ is the computed energy coming from a source at r_s recorded by a sensor at r_n. The variable ρ is the mass density of the plate, $c(\omega)$ is the group velocity of the waves over different angular frequencies ω up to Nyquist frequency ω_{Nyq}, $a(\omega)$ is the Fourier transform of the accelerometric recordings. $R(n) = ||r_n - r_s||$ is the distance between the source and the receiver, and h is the plate thickness. Depending on the plate material, there could be a viscous attenuation factor $e^{(2\gamma(\omega)R(n))}$ added to the right side of equation (1) to account for viscous energy losses where $\gamma(\omega)$ is the viscous attenuation inverse distance. However, for glass plates and the distances that are used in this experiment, viscous attenuation can be neglected (i.e., $\gamma \approx 0$, Farin et al., 2015). In the experimental setup, four sensors are placed on the bottom glass plate on different locations (see Figures 1b and 1c) to have a good spatial coverage. Standard deviation $\sigma(r_s)$ for source energy E_s at different test positions r_s on a regular grid for four different sensors are calculated. The minimum of this standard deviation over all tested positions r_s, indicates the source location (Turkaya et al., 2016). We used 5-mm grid spacing for the trial positions r_s on the 45 cm × 30 cm area covered by the porous medium inside the Hele-Shaw cell.

4. Image Processing for Deformation Localization

The optical images were captured via a high-speed camera (FastCam SA5-Photron, recorded with 125 or 1,000 fps with a resolution 1,024 × 1,024 pixels) during the experiments. These images are analyzed to localize the deformation corresponding to the time interval when the acoustic signal is emitted. The deformation of the medium during the acoustic emission leads time-lapse displacement fields of the porous medium (Chevalier et al., 2009; Eriksen et al., 2015, 2017, 2018; Niebling et al., 2010; Travelletti et al., 2012).

First, two successive images corresponding to the start and the end of the acoustic event is taken. Following this pretreatment, a digital image correlation (DIC) procedure, called Ncorr (an open source 2-D digital image correlation MATLAB software) is applied to obtain frame-to-frame displacement fields. Ncorr cross-correlates subwindows between two images to find displacement fields in between. A detailed description of Ncorr is given in Blaber et al. (2015).

In Figure 2a, an example of the displacement magnitude field obtained is given in the background. This map shows the magnitude of the absolute displacement of the medium (without any defined direction in the format of $||\bar{u}|| = \sqrt{u_x^2 + u_y^2}$ where $u_{x,y}$ are the displacements in directions x and y) occurring between two images taken at 8 ms apart. The grey-scale map shows the norm of the displacement field over the Hele-Shaw cell. As it can be seen for this snapshot, the displacements are localized near the fingertips. However, it is still possible to see nonzero displacements (of lower amplitudes) farther from the fingertips into the porous medium.

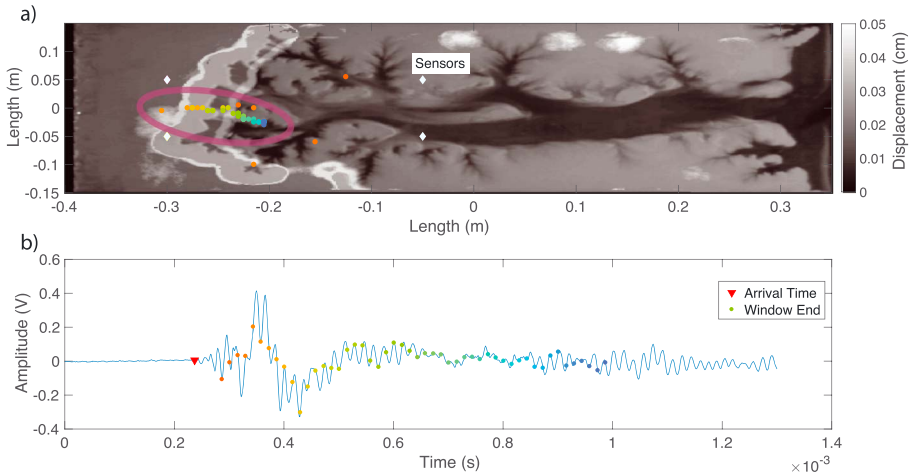

Figure 2. Localization of an acoustic event. (a) The localized source and receiver positions are indicated. Diamond markers show the accelerometer locations. The circle markers with different colors show the estimation of source energy homogeneity results with different input signal lengths starting from the red triangle at (b) and ending at the associated colored dot. The grayscale bar indicates the optically computed displacement magnitude in centimeter. (b) The acoustic event with different window sizes are presented. The red triangle shows the picked arrival time, which is the start of the signal for all time windows. The colored dots are the different ends of all windows used, resulting in different locations shown in (a).

5. Results and Discussion

In Figure 2 the localization for an acoustic event is given. Displacement maps (in gray) are overlaid by acoustic localization results. Markers with different colors are calculated for different time window lengths to define the primary signal (see supporting information, Figure S1 for window lengths). The size of the time window is set to extend stepwise to give multiple estimations for a single event for a better comparison with DIC results. DIC gives us an idea about the evolution of the signal location by indicating the location of the displacement that occurred during this time interval. In Figure 2 we see that the event source starts inside the porous medium and progresses toward the channel tips. Moreover, by increasing the size of the time window of the signal, we increase the sensitivity of the sensors for the waves coming from a larger area. The waves propagating on thin plates—similar to the glass plates which are used in this experimental study—may propagate at different velocities as a function of their frequency, which is the definition of dispersive waves. In this work, the dispersion of the Lamb Waves is taken into account in wave velocity calculations using experimental and theoretical computations (Royer & Dieulesaint, 2000).

In Figure 3, compared to the displacement magnitude given in Figure 2a we increased the temporal resolution to 1,000 frames per second instead of 125 fps. Moreover, to increase the spatial resolution of the images (and the resulting displacement maps) we are focusing on subparts of the Hele-Shaw cell where most of the grain displacement takes place. These settings allow us to follow the stick-slip events using the optical equipment with higher spatial and temporal resolution. In Figure 3(bottom) we see the location of the analyzed area in the cell (the channels are white, the granular porous medium is black, the analyzed part of the medium is gray).

Figure 3 also shows us how this stick-slip event starts inside the zone being compacted around 20 cm away from the tip of the channels with a decompacting zone behind. The pulse, pair of compacting zone and decompacting zone behind, travels backward toward the most advanced fingertip (in a direction opposite to the grains direction) and then gets distributed toward the tip of the channels. This is very similar to the phenomenon that we observed in Figure 2a where the source of the microseismic emission starts inside the porous medium and progresses toward the channel tips (see the circled zone). The first part of the signal is more sensitive to the start of the event than the whole slip event. Later on, the displacement gets distributed around most of the fingertips and ends up with the slip of the grains around the tips. The ESEH method is more sensitive to observe this evolution than the conventional arrival-time-based seismic location methods, since the arrival time of the event does not vary with time but the energy emitted per second does. As the time window gets enlarged, the sensors are more and more sensitive to signals coming from a larger area,

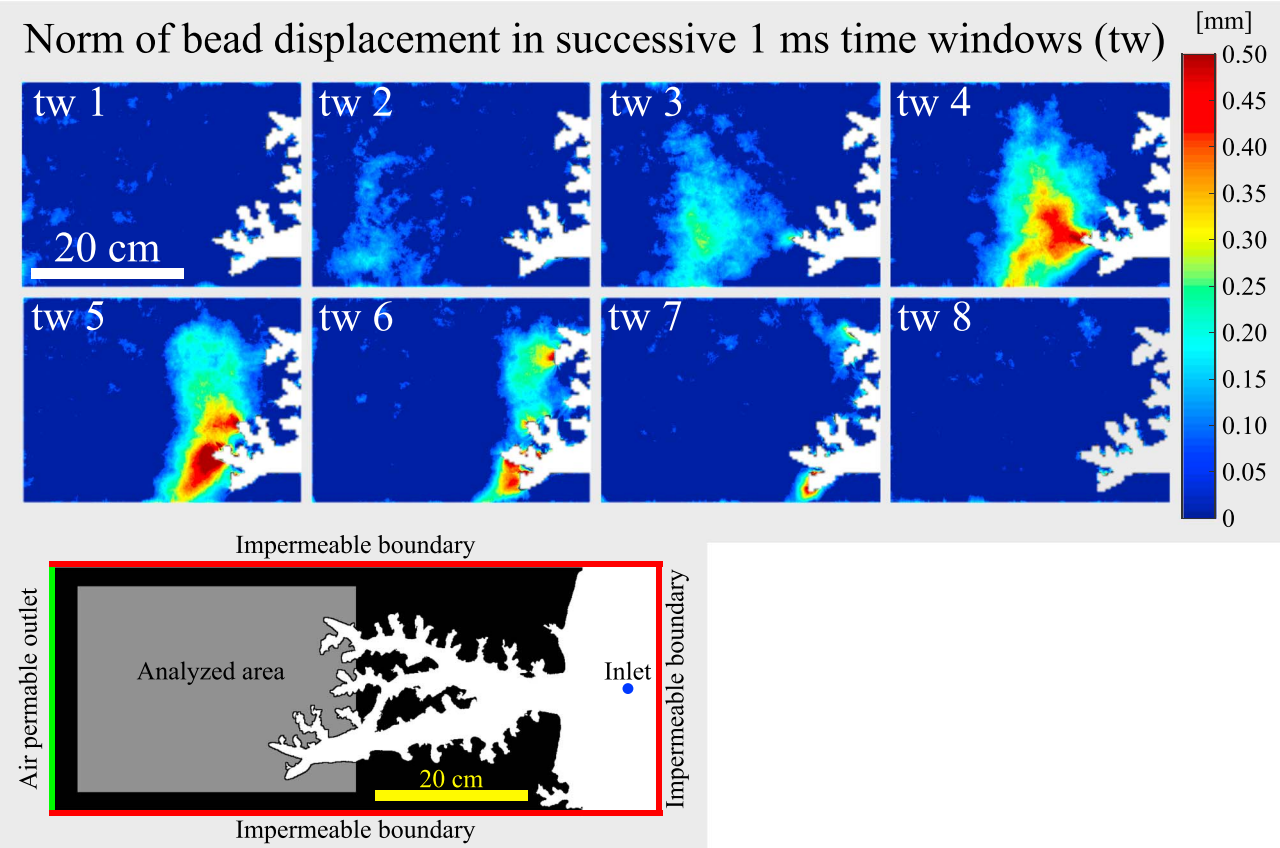

Figure 3. (top) Displacement magnitude (mm) in successive time windows (tw). The image set covers 8 ms. (b) Sketch of the Hele-Shaw cell and the location of the analyzed area.

and the resulting location, which assumes that the source is point-like, seems to come approximately from points belonging to the mobile region, closer to the fingertips.

6. Conclusion

In this article, we show that digital images and acoustic signals are very good (and coherent) monitoring tools to detect and localize fracturing and channeling in a porous medium. Different acoustic events having different natures (and locations) are investigated optically and acoustically (see Figures S5–S27 in the supporting information for more events and corresponding event recordings). The deformation magnitude maps obtained from digital image correlation method are compared with the acoustic signal based source localization results. The size of the time windows was set to extend freely so that the method would give multiple results for a single event for a better comparison. Depending on the polarization found on different sensors, it is possible to define the type of the source leading acoustic emissions. Localization results seem to fit well with displacement map obtained from the optical analysis techniques.

Acknowledgments
We would like to thank Alain Steyer and Miloud Talib for the technical support. This project has received funding from the European Union's Seventh Framework Programme for research under grant agreement 316889—FLOWTRANS, INSU ALEAS TelluS program, the International Associate Laboratory France-Norway on Deformation Flow and fracture of disordered Materials LIA D-FFRACT, from the Universities of Oslo and Strasbourg via a gjesteforsker program and an IDEX Espoirs award. Furthermore, this work was partly supported by the Research Council of Norway through its Centres of Excellence funding scheme, project 262644 and grant 213462/F20. The experimental data set and the Matlab routines used in this study can be found on this website (www.doi.org/10.5281/zenodo.1316548).

References

Accutech (1994). Accutech pneumatic fracturing extraction and hot gas injection phase one. Applications Analysis Report, DIANE Publishing Company.

Aki, K., & Richards, P. G. (2002). *Quantitative Seismology* (2nd ed.). South Orange, NJ: University Science Books.

Aochi, H., Poisson, B., Toussaint, R., & Schmittbuhl, J. (2011). Induced seismicity along a fault due to fluid circulation: Conception and application. Japan Geoscience Union Meeting 2011, May 2011, Makuhari, Chiba, Japan.

Blaber, J., Adair, B., & Antoniou, A. (2015). Ncorr: Open-source 2D digital image correlation Matlab software. *Experimental Mechanics*, *55*(6), 1105–1122.

Brandstein, M., Adcock, J., & Silverman, H. (1997). A closed-form location estimator for use with room environment microphone arrays. *IEEE, Speech and Audio Processing*, *5*(1), 45–50. https://doi.org/10.1109/89.554268

Candela, T., Wassing, B., Ter Heege, J., & Buijze, L. (2018). How earthquakes are induced. *Science*, *360*(6389), 598–600.

Charléty, J., Cuenot, N., Dorbath, L., Dorbath, C., Haessler, H., & Frogneux, M. (2007). Large earthquakes during hydraulic stimulations at the geothermal site of Soultz-sous-Forets. *International Journal of Rock Mechanics and Mining Sciences*, *44*(8), 1091–1105. https://doi.org/10.1016/j.ijrmms.2007.06.003

Chevalier, C., Lindner, A., Leroux, M., & Clément, E. (2009). Morphodynamics during air injection into a confined granular suspension. *Journal of Non-Newtonian Fluid Mechanics*, *158*(1), 63–72.

Christenson, B., Reyes, A., Young, R., Moebis, A., Sherburn, S., Cole-Baker, J., & Britten, K. (2010). Cyclic processes and factors leading to phreatic eruption events: Insights from the 25 September 2007 eruption through Ruapehu Crater Lake, New Zealand. *Journal of Volcanology and Geothermal Research*, *191*(1-2), 15–32.

Cornet, F. (2015). *Elements of crustal geomechanics*. Cambridge: Cambridge University Press.

Cornet, F., Helm, J., Poitrenaud, H., & Etchecopar, A. (1998). Seismic and aseismic slips induced by large-scale fluid injections. In S. Talebi (Ed.), *Seismicity Associated with Mines, Reservoirs and Fluid Injections* (pp. 563–583). Basel: Birkhäuser Basel.

Cuenot, N., Dorbath, C., & Dorbath, L. (2008). Analysis of the microseismicity induced by fluid injections at the EGS site of Soultz-sous-Forets (Alsace, France): Implications for the characterization of the geothermal reservoir properties. *Pure and Applied Geophysics*, *165*(5), 797–828. https://doi.org/10.1007/s00024-008-0335-7

Dorbath, L., Cuenot, N., Genter, A., & Frogneux, M. (2009). Seismic response of the fractured and faulted granite of Soultz-sous-Forets (France) to 5 km deep massive water injections. *Geophysical Journal International*, *177*, 653–675. https://doi.org/10.1111/j.1365-246X.2009.04030.x

Elnahrawy, E., Li, X., & Martin, R. (2004). The limits of localization using signal strength: A comparative study. IEEE, Sensor and Ad Hoc Communications and Networks, pp. 406–414, https://doi.org/10.1109/SAHCN.2004.1381942

Eriksen, F. K., Toussaint, R., Måløy, K. J., & Flekkøy, E. G. (2015). Invasion patterns during two-phase flow in deformable porous media. *Frontiers in Physics*, *3*, 81.

Eriksen, F. K., Toussaint, R., Turquet, A. L., Måløy, K. J., & Flekkøy, E. G. (2017). Pneumatic fractures in confined granular media. *Physical Review E*, *95*(062), 901. https://doi.org/10.1103/PhysRevE.95.062901

Eriksen, F. K., Toussaint, R., Turquet, A. L., Måløy, K. J., & Flekkøy, E. G. (2018). Pressure evolution and deformation of confined granular media during pneumatic fracturing. *Physical Review E*, *97*(012), 908. https://doi.org/10.1103/PhysRevE.97.012908

Farin, M., Mangeney, A., De Rosny, J., Toussaint, R., Sainte-Marie, J., & Shapiro, N. (2016). Experimental validation of theoretical methods to estimate the energy radiated by elastic waves during an impact. *Journal of Sound and Vibration*, *362*, 176–202.

Farin, M., Mangeney, A., Toussaint, R., de Rosny, J., Shapiro, N., Dewez, T., et al. (2015). Characterization of rockfalls from seismic signal: Insights from laboratory experiments. *Journal of Geophysical Research: Solid Earth*, *120*, 7102–7137. https://doi.org/10.1002/2015JB012331

Fehler, M., House, L., & Kaieda, H. (1987). Determining planes along which earthquakes occur: Method and application to earthquakes accompanying hydraulic fracturing. *Journal of Geophysical Research*, *92*(B9), 9407–9414. https://doi.org/10.1029/JB092iB09p09407

Fink, M. (2015). Acoustic imaging with time reversal methods: From medicine to NDT. *AIP Conference Proceedings*, *1650*(1), 13–23. https://doi.org/10.1063/1.4914591

Gao, F., Xie, H., Zhou, F., Ju, Y., Xie, L., Liu, Y., et al. (2014). Pneumatic fracturing method and system for exploiting shale gas. *US Patent Application*, *14*(335), 935.

Garnier, J., & Fink, M. (2015). Super-resolution in time-reversal focusing on a moving source. *Wave Motion*, *53*, 80–93. https://doi.org/10.1016/j.wavemoti.2014.11.005

Gershman, A., Turchin, V., & Zverev, V. (1995). Experimental results of localization of moving underwater signal by adaptive beamforming. *IEEE, Signal Processing*, *43*(10), 2249–2257. https://doi.org/10.1109/78.469863

Häring, M. O., Schanz, U., Ladner, F., & Dyer, B. C. (2008). Characterisation of the Basel 1 enhanced geothermal system. *Geothermics*, *37*(5), 469–495.

Hibert, C., Mangeney, A., Grandjean, G., & Nikolai, S. (2011). Slope instabilities in Dolomieu crater, Réunion Island: From seismic signals to rockfall characteristics. *Journal of Geophysical Research*, *116*, F04032. https://doi.org/10.1029/2011JF002038

Holland, A. A. (2013). Earthquakes triggered by hydraulic fracturing in South-Central Oklahoma. *Bulletin of the Seismological Society of America*, *103*(3), 1784. https://doi.org/10.1785/0120120109

Jamtveit, B., Ben-Zion, Y., Renard, F., & Austrheim, H. (2018). Earthquake-induced transformation of the lower crust. *Nature*, *556*(7702), 487–491. https://doi.org/10.1038/s41586-018-0045-y

Jolly, A., Jousset, P., Lyons, J., Carniel, R., Fournier, N., Fry, B., & Miller, C. (2014). Seismo-acoustic evidence for an avalanche driven phreatic eruption through a beheaded hydrothermal system: An example from the 2012 Tongariro eruption. *Journal of Volcanology and Geothermal Research*, *286*, 331–347. https://doi.org/10.1016/j.jvolgeores.2014.04.007

Kobchenko, M., Hafver, A., Jettestuen, E., Galland, O., Renard, F., Meakin, P., et al. (2013). Drainage fracture networks in elastic solids with internal fluid generation. *EPL (Europhysics Letters)*, *102*(6), 66002.

Malioutov, D., Cetin, M., & Willsky, A. (2005). A sparse signal reconstruction perspective for source localization with sensor arrays. *IEEE, Signal Processing*, *53*(8), 3010–3022. https://doi.org/10.1109/TSP.2005.850882

Manga, M., & Brodsky, E. (2006). Seismic triggering of eruptions in the far field: Volcanoes and geysers. *Annual Review of Earth and Planetary Sciences*, *34*, 263–291.

Niebling, M. J., Flekkøy, E. G., Måløy, K. J., & Toussaint, R. (2010). Mixing of a granular layer falling through a fluid. *Physical Review E-Statistical Nonlinear, and Soft Matter Physics*, *82*(1), 11301.

Oppenheimer, D. H. (1986). Extensional tectonics at the geysers geothermal area, california. *Journal of Geophysical Research*, *91*(B11), 11,463–11,476.

Peacock, M. (1996). Acoustic emission for detection of process-related damage in pressure vessels and piping. *Proceedings of the SPIE*, *2947*, 117–125. https://doi.org/10.1117/12.259158

Poland, M. P., Miklius, A., Sutton, A. J., & Thornber, C. R. (2012). A mantle-driven surge in magma supply to Kīlauea volcano during 2003–2007. *Nature Geoscience*, *5*(4), 295.

Rivalta, E., & Segall, P. (2007). Magma compressibility and the missing source for some dike intrusions. *Geophysical Research Letters*, *35*, L04306. https://doi.org/10.1029/2007GL032521

Royer, D., & Dieulesaint, E. (2000). *Elastic waves in solids I: Free and guided propagation*. Advanced Texts in Physics: Springer.

Schuring, J., Kosson, D., Fitzgerald, C., & Venkatraman, S. (1996). Pneumatic fracturing and multicomponent injection enhancement of in situ bioremediation. *US Patent 5*, *560*, 737.

Stanchits, S., Mayr, S., Shapiro, S., & Dresen, G. (2011). Fracturing of porous rock induced by fluid injection. Thermo-hydro-chemo-mechanical couplings in rock physics and rock mechanics. *Tectonophysics*, *503*(1), 129–145. https://doi.org/10.1016/j.tecto.2010.09.022

Sudo, Y., Ono, H., Hurst, A. W., Tsutsui, T., Mori, T., Nakaboh, M., et al. (1998). Seismic activity and ground deformation associated with 1995 phreatic eruption of Kuju Volcano, Kyushu, Japan. *Journal of Volcanology and Geothermal Research*, *81*(3), 245–267. https://doi.org/10.1016/S0377-0273(98)00011-0

Tazieff, H. (1989). Mechanisms of the Nyos carbon dioxide disaster and of so-called phreatic steam eruptions. *Journal of volcanology and geothermal research*, *39*(2-3), 109–116.

Terlizzi, J., & Minoo, J. (2009). Multi-touch display screen with localized tactile feedback. *US Patent Application*, *12*(069), 352.

Travelletti, J., Delacourt, C., Allemand, P., Malet, J.-P., Schmittbuhl, J., Toussaint, R., & Bastard, M. (2012). Correlation of multi-temporal ground-based optical images for landslide monitoring: Application, potential and limitations. *Journal of Photogrammetry and Remote Sensing*, *70*(0), 39–55. https://doi.org/10.1016/j.isprsjprs.2012.03.007

Turkaya, S., Toussaint, R., Eriksen, F. K., Lengliné, O., Daniel, G., Flekkøy, E. G., & Måløy, K. J. (2016). Note: Localization based on estimated source energy homogeneity. *Review of Scientific Instruments*, *87*(9), 96101.

Turkaya, S., Toussaint, R., Eriksen, F. K., Zecevic, M., Daniel, G., Flekkøy, E. G., et al. (2015). Bridging aero-fracture evolution with the characteristics of the acoustic emissions in a porous medium. *Frontiers in Physics*, *3*, 70.

Turquet, A. L., Toussaint, R., Eriksen, F. K., Daniel, G., Koehn, D., & Flekkøy, E. G. (2018). Microseismic emissions during pneumatic fracturing: A numerical model to explain the experiments. *Journal of Geophysical Research: Solid Earth*, *123*, 6922–6939. https://doi.org/10.1029/2017JB014613

Valin, J., Michaud, F., Rouat, J., & Letourneau, D. (2003). Robust sound source localization using a microphone array on a mobile robot. Proceedings 2003 IEEE/RSJ IROS (Vol. *2*, pp. 1228–1233). https://doi.org/10.1109/IROS.2003.1248813

Valkó, P., & Economides, M. (1995). *Hydraulic fracture mechanics*. Chichester: Wiley.

Zhu, Q., Tannenbaum, S., & Kurtzman, S. H. (2007). Optical tomography with ultrasound localization for breast cancer diagnosis and treatment monitoring. *Surgical Oncology Clinics of North America*, *16*(2), 307–321. https://doi.org/10.1016/j.soc.2007.03.008